

# Impacts of dark matter on the curvature of the neutron star

H. C. Das<sup>1,2</sup> <sup>★</sup>, Ankit Kumar<sup>1,2</sup> <sup>†</sup>, Bharat Kumar<sup>3</sup>, S. K. Biswal<sup>4</sup>, S. K. Patra<sup>1,2</sup>

<sup>1</sup> Institute of Physics, Sachivalya Marg, Bhubaneswar-751005, India

<sup>2</sup> Homi Bhabha National Institute, Training School Complex, Anushakti Nagar, Mumbai 400085, India

<sup>3</sup> Department of Physics & Astronomy, National Institute of Technology, Rourkela-769008, India

<sup>4</sup> Department of Astronomy, Xiamen University, Xiamen 361005, P. R. China

29 May 2022

## ABSTRACT

The effects of dark matter (DM) on the curvatures of the neutron star (NS) are examined by using the stiff and soft relativistic mean-field equation of states. The curvatures of the NSs are calculated with the variation of baryon density. Also, it is found that the radial variation of the different curvatures significantly affected by the presence of DM inside the NS. The effects of DM are less pronounced on the compactness of the maximum NS mass, but still significant. The NS surface curvature is found to be more remarkable for the massive star. The binding energy of the NSs become positive with the increasing DM momentum.

**Key words:** dark matter– equation of state– stars: neutron– curvature

## 1 INTRODUCTION

Neutron stars are the most known compact cosmological objects without event horizons (Shapiro & Teukolsky 1983; Lattimer & Prakash 2007) and its central density is 5–10 times the nuclear saturation density (Lattimer & Prakash 2004). It is the best ground for testing many astrophysical observations in the extreme gravitational field regime. However, a detailed study of the NS is not a settled issue yet due to its very complex structure. Its strong gravity may constraint or modify the equation of general relativity (GR) (Psaltis 2008; Will 2014). To explore the observables of the NS is quite tricky due to its uncertainty in the equation of state (EoS) at supra saturation density, mainly the symmetry energy (Tsang et al. 2009; Xu et al. 2010; Horowitz et al. 2014; Danielewicz & Lee 2014; Baldo & Burgio 2016; Li et al. 2019).

In August 2017, the LIGO and Virgo (Abbott et al. 2017) experiments found that the gravitational wave (GW) comes from the two NSs collision, and this unprecedented event opened a new era of astronomy, which is the deepest mystery of the Universe. In their observation, they have taken the Universe with no DM. We do not know the consequence about the DM on the GW due to its gravitationally attracting behaviour which bends the space-time curvature (Emspak 2017). The DM percentage is more than 80% (Joglekar et al. 2019) in the Universe so that the compact object when rotates around the centre in the Galaxy; it will sweep through DM halo and eventually capture some of the particles (Kouvaris 2008). The captured DM particles may have effects on the observational properties of NSs, which may use to constrain the nature of the DM, and also it curves the space-time which de-

pends on the percentage of DM contained inside the NS. The two things are capable of capturing the DM inside the NSs. First, its enormous gravitational force inside the NS. Second, the immense baryonic density inside the NS (Kouvaris 2008; Grijver et al. 2014).

Because of the uncertain nature of the DM, different DM particles like weakly interacting massive particle (WIMP), feebly interacting massive particle (FIMP) etc. are hypothesized. The WIMPs are the most abundant DM particles in the early Universe due to its freeze-out mechanism (Kouvaris & Tinyakov 2011; Ruppin et al. 2014). They equilibrated with the environments at freeze-out temperature and annihilated to form different standard model particles and leptons. Moreover, if the DM particles are annihilating, then it cools the old NSs (Kouvaris 2008; Ding et al. 2019; Bhat & Paul 2020). If the DM does not annihilate, then it interacts with baryon and also themselves, so that it affects the structure of the NS (De Lavallaz & Fairbairn 2010; Ciarcelluti & Sandin 2011). Once the DM contained inside the NS larger than the Chandrasekhar limit, it may form a mini black hole in the core, which can destroy the NSs (Kouvaris 2008). This mechanism can use to constrain the percentage of dark matter. Different approach has been used to calculated the NS properties with the inclusion of DM inside the NS (Sandin & Ciarcelluti 2009; De Lavallaz & Fairbairn 2010; Kouvaris & Tinyakov 2010; Ciarcelluti & Sandin 2011; Leung et al. 2011; Li et al. 2012; Panotopoulos & Lopes 2017; Ellis et al. 2018; Bhat & Paul 2020; Ivanytskyi et al. 2019; Das et al. 2019; Quddus et al. 2020; Das et al. 2020). However, in the present scenario, we use the non-annihilating WIMP as DM particle inside the NS. The detailed discussions can be found in our previous calculations (Das et al. 2020). As we know that the addition of DM softens the EoS, reduce mass-radius of the NS (Li et al.

<sup>★</sup> E-mail: harish.d@iopb.res.in

<sup>†</sup> ankit.k@iopb.res.in

2012; Das et al. 2019; Bhat & Paul 2020; Quddus et al. 2020; Das et al. 2020).

According to Einstein's, a massive body wraps the space-time and makes curvature around it and what we experience as gravity. Compactness parameter, which measures the strength of the gravitational field at a distance  $r$  from an object of mass  $M$  defined as  $\eta \equiv \frac{GM}{rc^2}$  and its values lie in between 0 and 1 (Psaltis 2008; He et al. 2015). The value of  $\eta = 0$  corresponding to flat Minkowski space in special relativity, while  $\eta = 1$  corresponds to the event horizon limit of a black hole, i.e. strongest gravitational field. The strength of the gravitational field is not due to the potential but due to the curvature (Psaltis 2008). So the curvature is the crucial thing to quantify gravity and the amount of wrapped in space-time. A massive body has larger curvature than the lighter one. Some experiments had already done to measure the curvature of the space-time. Recently, the direct detection of gravity-field curvature has done by using atom interferometers (Rosi et al. 2015).

We describe the different curvature quantities briefly in the concept of GR from the Ref. Carroll (2019). The Riemann tensor has twenty components in four dimensions. One cannot set all the components of the Riemann tensor to zero so that it is an appropriate tensor to measure the curvature. Since the Kretschmann scalar is the square root of the Riemann tensor, it also has the same property as Riemann tensor. The Ricci tensor is the contraction of the Riemann tensor, and the trace of the Ricci tensor is Ricci scalar or curvature scalar. One can say that the Ricci scalar and tensor contains all the information about the Riemann tensor leaving the traceless part of the Riemann tensor. If we remove all the contraction of Riemann tensor, then we have Weyl tensor. In the physical sense, the Ricci tensor and Ricci scalar measures the volumetric change of a body in the presence of the tidal effect. While, the Weyl tensor is telling about the distortion of the shape of the body, not its volume. However, the Riemann tensor measures both distortion of shape and volumetric change of the body in the presence of tidal force. In Ref. Ekşι et al. (2014) they have calculated the curvature of the NS, and they have noticed that GR is not well tested in the whole star than EoS and also found that the variation of Weyl tensor with the radius follows the power law for the large part of the star. Further, He et al. (2015) have taken both relativistic mean-field (RMF) and Skyrme-Hartree-Fock approaches and concluded that the symmetry energy has significant effects on the curvature of the lower mass NS and lesser effects on the massive NS. In the present work, we investigate the curvature of the NS in the presence of DM, with the different Lagrangian density of the models NL3 (Lalazissis et al. 1997), G3 (Kumar et al. 2017) and IOPB-I (Kumar et al. 2018).

It is exciting to probe the deeper inside the strong field regime of the NS by the modern observational instruments, and we may hope that the measurement of mass and radius of the NS more stringent constrain on the test of GR (Psaltis 2008). Till now, the accurate measurement of  $M$ - $R$  with minimal uncertainty is not done due to its unknown core. The density in the core is around 15 times the density at the surface (Ekşι et al. 2014). It means that the large mass is concentrated in the core. But the maximum mass and radius calculations are mainly from the unconstrained EoS regime. In contrary, the compactness and surface curvature are radially increasing towards the surface of the NS, which may be

the possibility to measure the maximum mass-radius that is more prominent for the EoS rather than the gravity. If we calculate the EoS in some way, but the application of GR to NS is difficult for all densities range. So that there will be the degeneracy breaking between the nuclear EoS and gravity models, which is a longstanding problem (Harada 1998; Sotani 2014; Ekşι et al. 2014). The detailed study requires for the EoS in a better way at supra saturation density. Since the GR equations breakdown at the strong-field regime, so we can either modify or extended up to some limit. In the Ref. Ekşι et al. (2014), it is quantified that the unconstrained gravity of the NS in the framework of GR. Moreover, to quantify the deviations come from GR in the strong-field regime, the detailed understanding required to study the properties of DM in the Universe (Psaltis 2008). Therefore, in the present calculations, we want to measure the curvature of the NS with the addition of DM using RMF approach.

In the present analysis, we take the RMF model to calculate the EoS. The RMF model reproduces the experimental value for exotic and super-heavy nuclei (Rashdan 2001; Bhuyan & Patra 2012) very well and gives a good description of the finite nuclei up to the  $\beta$ -stability line. The extended RMF (E-RMF) formalism (Kumar et al. 2017, 2018), which produced all the nuclear matter (NM) properties and satisfied the NSs observables calculated till now. In Sec. 2, we calculate the EoS of NS with the addition of DM. The curvature calculations are presented in 2.4. The detailed calculations are given in Ekşι et al. (2014). In Sec. 3, we present the variation of curvatures with the different quantities like baryon density, mass and radius with the addition of DM. The binding energy of the NS is also calculated with the inclusion of DM. Finally, we give a brief conclusion on the curvatures of the NS in Sec. 4.

## 2 FORMALISM

In this section, we provide the formalism required to compute the curvature of the NS in the presence of DM. First, we briefly sketch the E-RMF model along with DM by presenting model Lagrangian (Lalazissis et al. 1997; Kumar et al. 2017, 2018). All the parameters used in the E-RMF model were fitted to reproduce the observables of finite nuclei and infinite NM. The NS matter EoS is computed in the presence of DM and hence on the NS properties to solve the Tolman-Openheimer-Volkoff (TOV) equations and its different curvatures inside on it.

### 2.1 Construction of EoS using RMF approach

The RMF Lagrangian is built from the interaction of mesons-nucleons and their self ( $\sigma^2, \sigma^3, \sigma^4, \omega^2, \omega^4, \rho^2$  and  $\rho^4$ ) and cross-couplings ( $\sigma^2 - \omega^2, \omega^2 - \rho^2, \sigma - \omega^2$  and  $\sigma - \rho^2$ ) up to fourth order. The RMF Lagrangian is discussed in these Refs. (Miller & Green 1972; Serot & Walecka 1986; Furnstahl et al. 1987; Reinhard 1988; Ring 1996; Furnstahl et al. 1997; Kumar

et al. 2017, 2018). The RMF Lagrangian for NM system is

$$\begin{aligned}
\mathcal{L}_{nucl.} = & \sum_{\alpha=p,n} \bar{\psi}_\alpha \left\{ \gamma_\mu \left( i\partial^\mu - g_\omega \omega^\mu - \frac{1}{2} g_\rho \vec{\tau}_\alpha \cdot \vec{\rho}^\mu \right) - \left( M_{nucl.} \right. \right. \\
& \left. \left. - g_\sigma \sigma - g_\delta \vec{\tau}_\alpha \cdot \vec{\delta} \right) \right\} \psi_\alpha + \frac{1}{2} \partial^\mu \sigma \partial_\mu \sigma - \frac{1}{2} m_\sigma^2 \sigma^2 \\
& + \frac{\zeta_0}{4!} g_\omega^2 (\omega^\mu \omega_\mu)^2 - \frac{\kappa_3}{3!} \frac{g_\sigma m_\sigma^2 \sigma^3}{M_{nucl.}} - \frac{\kappa_4}{4!} \frac{g_\sigma^2 m_\sigma^2 \sigma^4}{M_{nucl.}^2} \\
& + \frac{1}{2} m_\omega^2 \omega^\mu \omega_\mu - \frac{1}{4} W^{\mu\nu} W_{\mu\nu} + \frac{\eta_1}{2} \frac{g_\sigma \sigma}{M_{nucl.}} m_\omega^2 \omega^\mu \omega_\mu \\
& + \frac{\eta_2}{4} \frac{g_\sigma^2 \sigma^2}{M_{nucl.}^2} m_\omega^2 \omega^\mu \omega_\mu + \frac{\eta_\rho}{2} \frac{m_\rho^2}{M_{nucl.}} g_\sigma \sigma \left( \vec{\rho}^\mu \cdot \vec{\rho}_\mu \right) \\
& + \frac{1}{2} m_\rho^2 \left( \vec{\rho}^\mu \cdot \vec{\rho}_\mu \right) - \frac{1}{4} \vec{R}^{\mu\nu} \cdot \vec{R}_{\mu\nu} - \Lambda_\omega g_\omega^2 g_\rho^2 (\omega^\mu \omega_\mu) \\
& \left. \left( \vec{\rho}^\mu \cdot \vec{\rho}_\mu \right) + \frac{1}{2} \partial^\mu \vec{\delta} \partial_\mu \vec{\delta} - \frac{1}{2} m_\delta^2 \vec{\delta}^2, \right. \quad (1)
\end{aligned}$$

where  $M_{nucl}$  (=939 MeV) is the mass of the nucleon.  $m_\sigma$ ,  $m_\omega$ ,  $m_\rho$  and  $m_\delta$  are the masses and  $g_\sigma$ ,  $g_\omega$ ,  $g_\rho$  and  $g_\delta$  are the coupling constants for the  $\sigma$ ,  $\omega$ ,  $\rho$  and  $\delta$  mesons respectively.  $\kappa_3$  (or  $\kappa_4$ ) and  $\zeta_0$  are the self-interacting coupling constants of the  $\sigma$  and  $\omega$  mesons respectively.  $\eta_1$ ,  $\eta_2$ ,  $\eta_\rho$  and  $\Lambda_\omega$  are the coupling constants of non-linear cross-coupled terms. The quantities  $W^{\mu\nu}$  and  $\vec{R}^{\mu\nu}$  being the field strength tensors for the  $\omega$  and  $\rho$  mesons respectively, defined as  $W^{\mu\nu} = \partial^\mu \omega^\nu - \partial^\nu \omega^\mu$  and  $\vec{R}^{\mu\nu} = \partial^\mu \vec{\rho}^\nu - \partial^\nu \vec{\rho}^\mu$ . The  $\vec{\tau}$  are the Pauli matrices and behave as the isospin operator. Parameters and saturation properties for NL3 (Lalazissis et al. 1997), G3 (Kumar et al. 2017) and IOPB-I (Kumar et al. 2018) along with the empirical/experimental values are given in Table 1.

The meson fields for the NM system are calculated by solving the mean-field equation of motions (Kumar et al. 2017, 2018; Das et al. 2019) in a self-consistent way. The energy density ( $\mathcal{E}_{nucl.}$ ) and pressure ( $P_{nucl.}$ ) are calculated using the energy-momentum stress-tensor technique which is given by (Walecka 1974; Glendenning 1997)

$$\begin{aligned}
\mathcal{E}_{nucl.} = & \frac{\gamma}{(2\pi)^3} \sum_{i=p,n} \int_0^{k_i} d^3 k E_i^\star(k_i) + \rho_b W + \frac{1}{2} \rho_3 R \\
& + \frac{m_s^2 \Phi^2}{g_s^2} \left( \frac{1}{2} + \frac{\kappa_3}{3!} \frac{\Phi}{M_{nucl.}} + \frac{\kappa_4}{4!} \frac{\Phi^2}{M_{nucl.}^2} \right) - \frac{1}{4!} \frac{\zeta_0 W^4}{g_\omega^2} \\
& - \frac{1}{2} m_\omega^2 \frac{W^2}{g_\omega^2} \left( 1 + \eta_1 \frac{\Phi}{M_{nucl.}} + \frac{\eta_2}{2} \frac{\Phi^2}{M_{nucl.}^2} \right) \\
& - \Lambda_\omega (R^2 \times W^2) - \frac{1}{2} \left( 1 + \frac{\eta_\rho \Phi}{M_{nucl.}} \right) \frac{m_\rho^2}{g_\rho^2} R^2 \\
& + \frac{1}{2} \frac{m_\delta^2}{g_\delta^2} D^2, \quad (2)
\end{aligned}$$

**Table 1.** The parameter sets NL3 (Lalazissis et al. 1997), G3 (Kumar et al. 2017) and IOPB-I (Kumar et al. 2018) are listed. All the coupling constants are dimensionless, except  $k_3$  which is in  $\text{fm}^{-1}$ . The NM parameters are given at saturation point for NL3, G3 and IOPB-I parameter sets in the lower panel. The empirical/experimental values for NM parameters are also given at the saturation density. The references are [a],[b], [c] & [d] (Zyla et al. 2020), [e]&[f] (Bethe 1971), [g] (Garg & Colas 2018), [h]&[i] (Danielewicz & Lee 2014), and [j] (Zimmerman et al. 2020).

Parameter	NL3	G3	IOPB-I	Empirical/Expt. Value
$m_\sigma/M_{nucl.}$	0.541	0.559	0.533	0.426 – 0.745 [a]
$m_\omega/M_{nucl.}$	0.833	0.832	0.833	0.833 – 0.834 [b]
$m_\rho/M_{nucl.}$	0.812	0.820	0.812	0.825 – 0.826 [c]
$m_\delta/M_{nucl.}$	0.0	1.043	0.0	1.022 – 1.064 [d]
$g_\sigma/4\pi$	0.813	0.782	0.827	
$g_\omega/4\pi$	1.024	0.923	1.062	
$g_\rho/4\pi$	0.712	0.962	0.885	
$g_\delta/4\pi$	0.0	0.160	0.0	
$k_3$	1.465	2.606	1.496	
$k_4$	-5.688	1.694	-2.932	
$\zeta_0$	0.0	1.010	3.103	
$\eta_1$	0.0	0.424	0.0	
$\eta_2$	0.0	0.114	0.0	
$\eta_\rho$	0.0	0.645	0.0	
$\Lambda_\omega$	0.0	0.038	0.024	
$\rho_0 (\text{fm}^{-3})$	0.148	0.148	0.149	0.148 – 0.185 [e]
$BE(\text{MeV})$	-16.29	-16.02	-16.10	-15.00 – 17.00 [f]
$K(\text{MeV})$	271.38	243.96	222.65	220 – 260 [g]
$J(\text{MeV})$	37.43	31.84	33.30	30.20 – 33.70 [h]
$L(\text{MeV})$	118.65	49.31	63.58	35.00 – 70.00 [i]
$K_{sym}(\text{MeV})$	101.34	-106.07	-37.09	-174 – -31 [j]
$Q_{sym} (\text{MeV})$	177.90	915.47	862.70	—

$$\begin{aligned}
P_{nucl.} = & \frac{\gamma}{3(2\pi)^3} \sum_{i=p,n} \int_0^{k_i} d^3 k \frac{k^2}{E_i^\star(k_i)} + \frac{1}{4!} \frac{\zeta_0 W^4}{g_\omega^2} \\
& - \frac{m_s^2 \Phi^2}{g_s^2} \left( \frac{1}{2} + \frac{\kappa_3}{3!} \frac{\Phi}{M_{nucl.}} + \frac{\kappa_4}{4!} \frac{\Phi^2}{M_{nucl.}^2} \right) \\
& + \frac{1}{2} m_\omega^2 \frac{W^2}{g_\omega^2} \left( 1 + \eta_1 \frac{\Phi}{M_{nucl.}} + \frac{\eta_2}{2} \frac{\Phi^2}{M_{nucl.}^2} \right) \\
& + \Lambda_\omega (R^2 \times W^2) + \frac{1}{2} \left( 1 + \frac{\eta_\rho \Phi}{M_{nucl.}} \right) \frac{m_\rho^2}{g_\rho^2} R^2 \\
& - \frac{1}{2} \frac{m_\delta^2}{g_\delta^2} D^2. \quad (3)
\end{aligned}$$

Where  $\Phi$ ,  $W$ ,  $R$  and  $D$  are the redefined fields for  $\sigma$ ,  $\omega$ ,  $\rho$  and  $\delta$  mesons as  $\Phi = g_s \sigma^0$ ,  $W = g_\omega \omega^0$ ,  $R = g_\rho \vec{\rho}^0$  and  $D = g_\delta \delta^0$  respectively. The  $E_i^\star(k_i) = \sqrt{k_i^2 + M_i^\star{}^2}$ , where  $M_i^\star$  is the effective mass and  $k_i$  is the momentum of the nucleon and  $\gamma$  is the spin degeneracy factor which is equal to 2 for individual nucleons.

Inside the NS, many particles like hyperons, nucleons and leptons are present. The neutron decays to proton, electron and anti-neutrino inside the NS (Glendenning 1997). This process is called as  $\beta$ -decay. To maintain the charge neutrality condition, the inverse  $\beta$ -decay process occurred. The

process can be expressed as

$$\begin{aligned} n &\rightarrow p + e^- + \bar{\nu}, \\ p + e^- &\rightarrow n + \nu. \end{aligned} \quad (4)$$

To maintain the stability of NSs, there must have both  $\beta$ -equilibrium and charge-neutrality conditions, which are expressed in term of chemical potential

$$\begin{aligned} \mu_n &= \mu_p + \mu_e, \\ \mu_e &= \mu_\mu, \\ \mu_p &= \mu_e + \mu_\mu. \end{aligned} \quad (5)$$

Where  $\mu_n$ ,  $\mu_p$ ,  $\mu_e$ , and  $\mu_\mu$  are the chemical potentials of neutrons, protons, electrons, and muons, respectively. When the chemical potential of electron is equal to the muon rest mass, then muon appear inside the NS. The chemical potentials  $\mu_n$ ,  $\mu_p$ ,  $\mu_e$ , and  $\mu_\mu$  are given by (Das et al. 2020)

$$\mu_{n,p} = g_\omega \omega_0 \pm g_\rho \rho_0 \mp g_\delta \delta_0 + \sqrt{k_{n,p}^2 + (M_{n,p}^\star)^2}, \quad (6)$$

$$\mu_{e,\mu} = \sqrt{k_{e,\mu}^2 + m_{e,\mu}^2}, \quad (7)$$

where  $M_n^\star$  and  $M_p^\star$  are the effective mass of neutron and proton respectively. The particle fraction inside the NS is calculated by solving Eq. (5) using the Eqs. (6 – 7) for a given baryon density by self-consistently. The energy density and pressure of NS are given by,

$$\begin{aligned} \mathcal{E}_{NS} &= \mathcal{E}_{nucl.} + \mathcal{E}_l, \\ \text{and} \quad P_{NS} &= P_{nucl.} + P_l, \end{aligned} \quad (8)$$

where,

$$\mathcal{E}_l = \sum_{l=e,\mu} \frac{2}{(2\pi)^3} \int_0^{k_l} d^3k \sqrt{k^2 + m_l^2}, \quad (9)$$

and

$$P_l = \sum_{l=e,\mu} \frac{2}{3(2\pi)^3} \int_0^{k_l} \frac{d^3k}{\sqrt{k^2 + m_l^2}} \frac{k^2}{k^2 + m_l^2}. \quad (10)$$

Where  $\mathcal{E}_l$ ,  $P_l$  and  $k_l$  are the energy density, pressure and Fermi momentum for leptons respectively. The Eq. (8) gives the total energy, pressure of the NS.

## 2.2 Interaction of DM candidates in NS

DM particles accreted inside the NS core due to its high gravitational field (Goldman & Nussinov 1989; Kouvaris 2008; Xiang et al. 2014; Das et al. 2019) and the amount of accreted DM depends directly on its evolving life time. In this scenario, we consider the Neutralino (Martin 1998; Panotopoulos & Lopes 2017; Das et al. 2019, 2020) as a fermionic DM candidate which interacts with nucleon via SM Higgs. The detailed formalism has been taken from our previous analysis (Das et al. 2020) and the total Lagrangian is written as:

$$\begin{aligned} \mathcal{L}_{tot.} &= \mathcal{L}_{NS} + \bar{\chi} [i\gamma^\mu \partial_\mu - M_\chi + yh] \chi + \frac{1}{2} \partial_\mu h \partial^\mu h \\ &\quad - \frac{1}{2} M_h^2 h^2 + f \frac{M_{nucl.}}{v} \bar{\varphi} h \varphi, \end{aligned} \quad (11)$$

where  $\mathcal{L}_{NS}$  is the NS Lagrangian and  $\varphi$  and  $\chi$  are the nucleonic and DM wave functions respectively.  $h$  is the Higgs field.

All the parameters value like  $y (= 0.07)$ ,  $f (= 0.35)$  and  $v (= 246$  GeV) are given in (Das et al. 2020). From the Lagrangian in Eq. (11), we get the total energy density ( $\mathcal{E}_{tot.}$ ) and pressure ( $P_{tot.}$ ) for NS with DM given as (Das et al. 2020)

$$\begin{aligned} \mathcal{E}_{tot.} &= \mathcal{E}_{NS} + \frac{2}{(2\pi)^3} \int_0^{k_f^{DM}} d^3k \sqrt{k^2 + (M_\chi^\star)^2} \\ &\quad + \frac{1}{2} M_h^2 h_0^2, \end{aligned} \quad (12)$$

$$\begin{aligned} P_{tot.} &= P_{NS} + \frac{2}{3(2\pi)^3} \int_0^{k_f^{DM}} \frac{d^3k}{\sqrt{k^2 + (M_\chi^\star)^2}} \\ &\quad - \frac{1}{2} M_h^2 h_0^2, \end{aligned} \quad (13)$$

where  $k_f^{DM}$  is the DM Fermi momentum. The  $M_{n,p}^\star$  and  $M_\chi^\star$  are the effective masses of nucleon and DM, which are given as

$$\begin{aligned} M_{n,p}^\star &= M_{nucl.} + g_\sigma \sigma_0 \mp g_\delta \delta_0 - \frac{f M_{nucl.}}{v} h_0, \\ M_\chi^\star &= M_\chi - y h_0, \end{aligned} \quad (14)$$

where the  $\sigma_0$ ,  $\delta_0$  and  $h_0$  are the field for  $\sigma$ ,  $\delta$  and Higgs respectively.

## 2.3 Mass and Radius of the NS

Here we calculate the NS observables like  $M$  and  $R$  etc. using TOV equations. Hence, we take the EoSs of NS with DM and input to the TOV equations (Tolman 1939; Oppenheimer & Volkoff 1939) are given as

$$\frac{dP_{tot.}(r)}{dr} = - \frac{(P_{tot.}(r) + \mathcal{E}_{tot.}(r))(m(r) + 4\pi r^3 P_{tot.}(r))}{r(r - 2m(r))}, \quad (15)$$

and

$$\frac{dm(r)}{dr} = 4\pi r^2 \mathcal{E}_{tot.}(r), \quad (16)$$

where  $\mathcal{E}_{tot.}(r)$  and  $P_{tot.}(r)$  are the total energy and pressure density as a function of radial distance.  $m(r)$  is the gravitational mass, and  $r$  is the radial parameter. These two coupled equations are solved to get the mass and radius of the NS at certain central density.

## 2.4 Mathematical formulation for different curvatures

We adopt the mathematical form of different curvature quantities from Ekşioğlu et al. (2014), which measure the space-time curvature for both inside and outside the compact objects. Several curvatures are Riemann tensor, Ricci tensor, Ricci scalar and Weyl tensor, which are given as

The Ricci scalar

$$\mathcal{R}(r) = 8\pi \left[ \mathcal{E}_{tot.}(r) - 3P_{tot.}(r) \right], \quad (17)$$

the full contraction of the Ricci tensor

$$\mathcal{J}^2(r) \equiv \mathcal{R}_{\mu\nu} \mathcal{R}^{\mu\nu} = (8\pi)^2 \left[ \mathcal{E}_{tot.}^2(r) + 3P_{tot.}^2(r) \right], \quad (18)$$

the Kretschmann scalar (full contraction of the Riemann tensor)

$$\begin{aligned} \mathcal{K}^2(r) &= \mathcal{R}^{\mu\nu\rho\sigma}\mathcal{R}_{\mu\nu\rho\sigma} \\ &= (8\pi)^2[3\mathcal{E}_{tot.}^2(r) + 3P_{tot.}^2(r) + 2P_{tot.}(r)\mathcal{E}_{tot.}(r)] \\ &\quad - \frac{128\mathcal{E}_{tot.}(r)m(r)}{r^3} + \frac{48m^2(r)}{r^6}, \end{aligned} \quad (19)$$

and the full contraction of the Weyl tensor

$$W^2(r) \equiv C^{\mu\nu\rho\sigma}C_{\mu\nu\rho\sigma} = \frac{4}{3}\left(\frac{6m(r)}{r^3} - 8\pi\mathcal{E}_{tot.}(r)\right)^2. \quad (20)$$

Where  $\mathcal{E}_{tot.}$ ,  $P_{tot.}$ ,  $m(r)$  and  $r$  are the energy density, pressure, mass and radius of the NS respectively. At the surface  $m \rightarrow M$  and  $r \rightarrow R$ . The Ricci tensor and Ricci scalar vanishing outside the NSs because all tensors depend on the  $\mathcal{E}_{tot.}(r)$ ,  $P_{tot.}(r)$  and  $m(r)$ , which are zero outside the star. There is a non-vanishing component of the Riemann tensor which does not vanish;  $\mathcal{R}^1_{010} = -\frac{2M}{R^3} = -\xi$ , even in the outside of the star (Eksi et al. 2014; He et al. 2015). So the Riemann tensor is the more relevant to measure the curvature of the NSs than others.

## 3 RESULTS AND DISCUSSION

### 3.1 Choice of parameter sets

In the present work, three sets of parameter are chosen, namely NL3 (Lalazissis et al. 1997), IOPB-I (Kumar et al. 2018) and G3 (Kumar et al. 2017). The NL3 parameter set corresponds to the standard RMF model, which contains non-linear interactions (self-interaction of the sigma meson). It has relatively high incompressibility in comparison to the other two parameter sets. The NM properties of all the three-parameter sets are given in Table 1. In the case of IOPB-I, there are two extra coupling parameters,  $\Lambda_\omega$  and  $\zeta_0$  are taken on top of the NL3 parameter set. These two coupling parameters play a vital role in both finite and infinite NM system (Singh et al. 2014; Biswal et al. 2015; Kumar et al. 2018). The parameter  $\Lambda_\omega$  controls the symmetry energy (or neutron skin thickness of finite nuclei) as well as the maximum mass of the NS (Horowitz & Piekarewicz 2001).  $\zeta_0$ , which is the coupling constants for the self-interaction of the vector-meson, affects the EoS at higher density (Sugahara & Toki 1994; Mäijller & Serot 1996). So it is imperative to include for the study of the NS physics. The interaction G3 corresponds to the complete E-RMF Lagrangian, as discussed in Sec. 2.1. One can note that G3 parameter has extra six couplings constants ( $\eta_1$ ,  $\eta_2$ ,  $\eta_\rho$ ,  $g_\delta$ ,  $\Lambda_\omega$  and  $\zeta_0$ ) in compare to the NL3 parameter set. All the couplings constants of the Lagrangian in Eq. (1) are obtained by fitting the several properties of finite nuclei and infinite NM at saturation density. The NL3 being the stiffest EoS enrich with the higher NS mass ( $2.774 M_\odot$ ) in comparison to other parameter sets. The maximum mass is given by IOPB-I ( $2.149 M_\odot$ ) is closer to the one suggested by the Cromartie et al. (2019) along with the calculated values of canonical radius and tidal deformability are in accordance with the GW170817 (Abbott et al. 2017, 2018). We have given the results with these parameter sets, for the comparative study and better understanding of the parametric dependency of the dark matter effects on the curvatures of the neutron star.

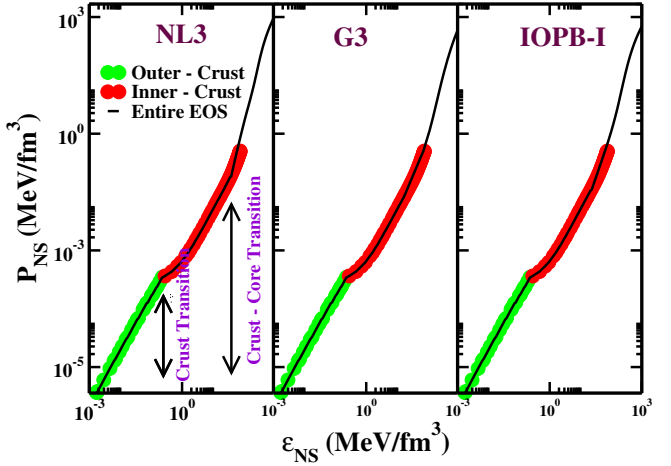


**Figure 1.** (colour online) The EoS of the NS is shown for different parameter sets for core part ( $<5\rho_0$ ), where  $\rho_0$  is the NM saturation density. The red and green shaded line represents the inner crust ( $3 \times 10^{-4} - 8 \times 10^{-2} \text{ fm}^{-3}$ ) and outer crust ( $6 \times 10^{-12} - 2.61 \times 10^{-4} \text{ fm}^{-3}$ ) of Ref. (Sharma et al. 2015)

### 3.2 Equation of State

EoS is the most vital equipment to understand the properties of the NS. We use different EoS emerged from different parameter sets like NL3 (Lalazissis et al. 1997), G3 (Kumar et al. 2017) and IOPB-I (Kumar et al. 2018) to explore the curvature of NS. The calculated EoS in Eqs. (8) is only for the core part of the NS and it is different for NL3, G3 and IOPB-I parameter sets. However, for the crust part (both inner and outer crust), we adopt the Sharma et. al. EoS (Sharma et al. 2015) which added to form unified EoS for the whole density range. The entire EoS depicted in Fig. 1. Moreover, we have found in our recent work Das et al. (2020) that the EoS becomes softer with the addition of DM and reduces the  $M$  and  $R$  of the NS. The maximum masses, radii and its corresponding central densities are given in Table 2 for different DM momenta.

### 3.3 Contribution to curvatures by various parameters

We calculate various curvatures like  $\mathcal{K}$ ,  $\mathcal{J}$ ,  $\mathcal{R}$  and  $\mathcal{W}$  of the NS in the presence of DM. NS has different density regions like the inner core, inner crust and an outer crust (see Fig. 1). The core part is the most crucial component of the star, which account the density in the range of 5-10 times of the nuclear saturation density (Lattimer & Prakash 2004). Here, we calculate the curvature of the NS with the variation of the baryon density with different DM momentum for different parameter sets, which is shown in Fig. 2. The curvatures are increasing or decreasing with the increase of the baryon density. It is observed that at lower density the quantity  $\mathcal{K}$  and  $\mathcal{W}$  give higher curvature than  $\mathcal{J}$ ,  $\mathcal{R}$ . Near to the surface, the curvatures  $\mathcal{J}$ , and  $\mathcal{R}$  are almost vanished due to their zero vacuum expectation value. The  $\mathcal{K}$  and  $\mathcal{W}$  approach each other at the radius of the crust and have a local maximum in that region. Therefore, the crust region is the best site to measure the deviation of GR in the strong gravity regime,

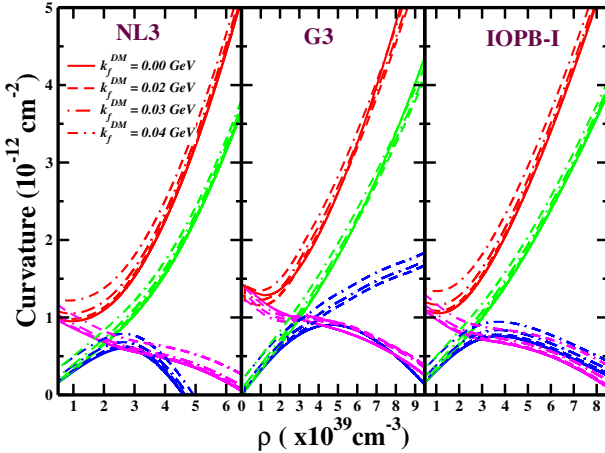


**Figure 2.** (colour online) The variation of different curvatures  $\mathcal{K}$  (red),  $\mathcal{J}$  (green),  $\mathcal{R}$  (blue) and  $\mathcal{W}$  (magenta) with baryon density for NL3 (left), G3 (middle) and IOPB-I (right) in the presence of DM for corresponding maximum mass.

the activity of the pulsar glitches, and the modulation of the cooling of NS (Eksi et al. 2014).

The radial variation of the curvatures is shown in Fig. 3 with the addition of DM. It is found that in the presence of DM, the curvatures of the NS increase with the increasing of  $k_f^{DM}$ . All the curvatures are maximum at the centre of the star except Weyl tensor. However, the Ricci scalar is negative within the star (for maximum mass), as shown in Fig. 3, whose magnitude is higher for stiffer EoS like NL3 than others two G3 and IOPB-I. At the surface of the star,  $\mathcal{E}_{tot.} = 0$ ,  $P_{tot.} = 0$ , so  $\mathcal{K}$  and  $\mathcal{W}$  are equal to  $\frac{4\sqrt{3}M}{R^3}$  from Eqs. (19) and (20). Near the surface of the NS, the  $\mathcal{J}$  and  $\mathcal{R}$  are approach to zero. If we assume that the NS has uniform density, i.e.  $m = \frac{4}{3}\pi r^3 \rho$ , then the Eq. (20) is equal to zero. Therefore, the  $\mathcal{W}$  tends to zero at the core. As we approach from outer crust to the surface, the density in this region is like diffuse state. So that  $\mathcal{W}$  is maximum at the surface. Various curvatures follow the similar radial variation in the presence of the DM, but the magnitude of the curvature increases.

The compactness parameter measures the degree of density of the star. The NS has a larger mass and smaller radius as compared to the Sun, so its compactness is  $10^5$  times larger than our Sun. Therefore, we study the radial variation of the compactness of the NS in the presence of the DM, which is depicted in Fig. 4. The compactness within the star increases with the increase of the DM momentum for different parameter sets, which is shown in Fig. 4. It has a larger value for the maximum mass NS in compare to the canonical star. With the increase of the DM percentage, the EoS becomes softer, which has less compactness as compared to the stiff EoS.

We calculate the  $\mathcal{K}(r)$  within the NS. To see the parametric dependence of the curvature with different radius, we fix the DM percentage (0.04 GeV), which is shown in Fig. 5 for different masses of the star. If one see carefully, the radial variation of the  $\mathcal{K}(r)$  increases slowly with different mass star up to canonical mass; then the percentage is increasing for the maximum mass star. With the addition of DM, the change  $\mathcal{K}(r)$  increases  $\approx 33\%$ , and this percentage is more for maximum mass star. It is observed that the softer EoS, namely G3, has larger curvature than stiffer like NL3 and IOPB-I

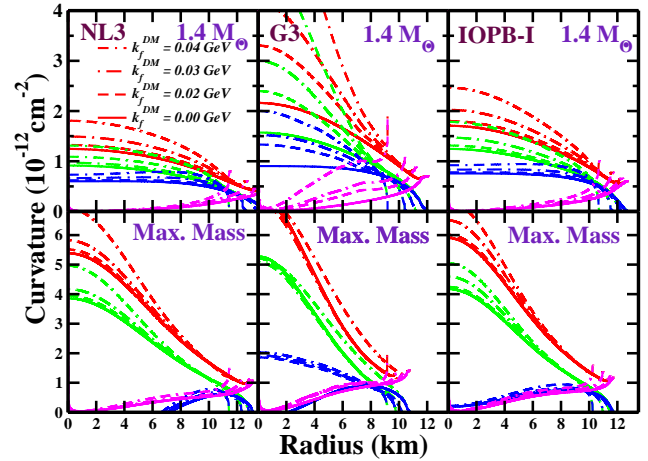


**Figure 3.** (colour online) The radial variation of all the curvatures  $\mathcal{K}$  (red),  $\mathcal{J}$  (green),  $\mathcal{R}$  (blue) and  $\mathcal{W}$  (magenta) for NL3 (left), G3 (middle) and IOPB-I (right) in the presence of DM.

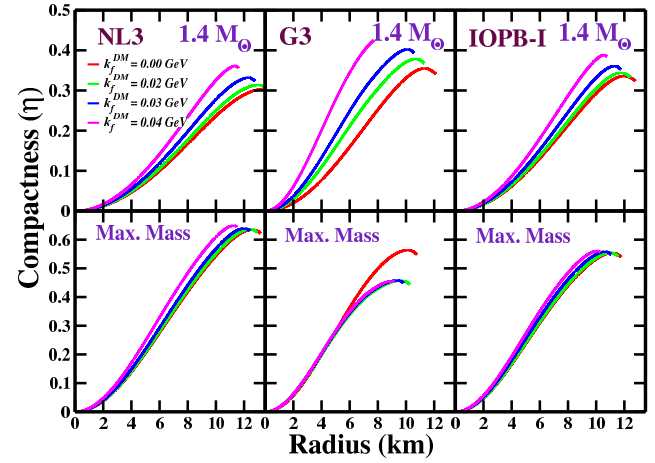


**Figure 4.** (colour online) The radial variation of compactness ( $\eta$ ) for NL3 (left), G3 (middle) and IOPB-I (right) in the presence of DM.

both for the canonical and maximum mass star. Hence, we conclude that the effects of DM on the curvature of the NS changes considerably not only on the  $\mathcal{K}$  but also on the  $\mathcal{J}$ ,  $\mathcal{R}$ ,  $\mathcal{W}$ .

Here, we calculate the curvature at the surface of the NS, which is more prominent to quantify the space-time wrap in the Universe. The variation of  $\mathcal{K}(R)/\mathcal{K}_\odot$  with the mass of the NS is shown in Fig. 6. The curvature ( $\mathcal{K}_\odot$ ) and compactness ( $\eta_\odot$ ) at the surface of the sun are  $3.06 \times 10^{-27} \text{ cm}^{-2}$  and  $4.27 \times 10^{-6}$  respectively (Eksi et al. 2014). In our calculations, it is found that the surface curvature for NS without DM are

**Table 2.** The central density  $\mathcal{E}_c$ , mass  $M$  ( $M_\odot$ ), radius  $R$ , Surface curvature  $\mathcal{K}(R)$ , binding energy  $B/M$  of the NS are tabulated with the variation of  $k_f^{DM}$  both for canonical ( $1.4 M_\odot$ ) and maximum mass star for NL3, G3 and IOPB-I parameter sets.

$k_f^{DM}$ (GeV)	Star type	$\mathcal{E}_c$			$M$			$R$			$\mathcal{K}(R)$			$B/M$		
		(MeV fm $^{-3}$ )			( $M_\odot$ )			(km)			$(10^{14} \mathcal{K}_\odot)$					
		NL3	G3	IOPB-I	NL3	G3	IOPB-I	NL3	G3	IOPB-I	NL3	G3	IOPB-I	NL3	G3	IOPB-I
0.00	Canonical	270	460	366	1.400	1.400	1.400	14.08	12.11	12.78	1.477	2.320	1.977	-0.084	-0.098	-0.092
	Maximum	870	1340	1100	2.774	1.997	2.149	13.16	10.78	11.76	3.584	4.695	3.894	-0.207	-0.162	-0.165
0.02	Canonical	286	700	385	1.400	1.400	1.400	13.63	11.32	12.42	1.626	2.841	2.153	-0.038	-0.065	-0.057
	Maximum	890	1440	1120	2.734	1.543	2.118	12.91	10.25	11.54	3.741	4.218	4.061	-0.178	-0.071	-0.139
0.03	Canonical	320	870	430	1.400	1.400	1.400	12.78	10.56	11.75	1.976	3.515	2.546	0.045	-0.011	0.016
	Maximum	940	1480	1190	2.646	1.491	2.050	12.39	9.81	11.06	4.097	4.651	4.492	-0.116	-0.024	-0.009
0.04	Canonical	383	1470	518	1.400	1.400	1.400	11.60	9.18	10.76	2.638	6.365	3.317	0.016	0.055	0.105
	Maximum	1100	1500	1390	2.502	1.402	1.937	11.46	9.15	10.23	4.093	6.478	5.341	-0.023	-0.001	-0.002

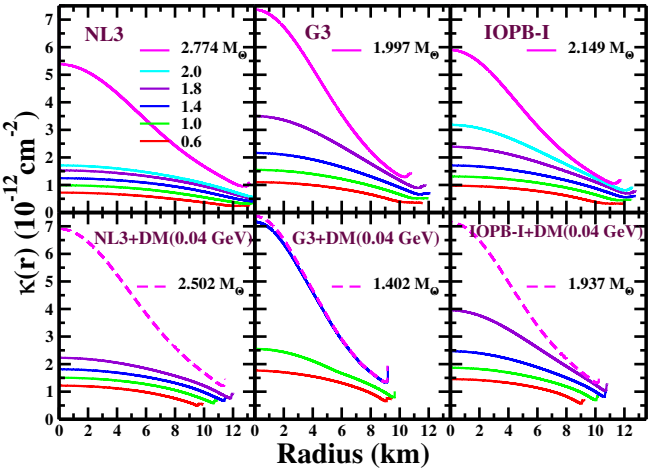


**Figure 5.** (colour online) The radial variation of  $\mathcal{K}(r)$  without and with DM having momentum 0.04 GeV. The corresponding maximum mass is shown bold line (without DM) and dashed-line (with DM).

3.584, 4.695 and 3.894, with DM momentum 0.04 GeV these values are 4.093, 6.478 and 5.341 for NL3, G3, and IOPB-I parameter sets respectively. The comparison of our results with the sun gives the  $\mathcal{K}(R)/\mathcal{K}_\odot \approx 10^{14}$  and  $\eta/\eta_\odot \approx 10^5$  respectively. The ratio  $\mathcal{K}(R)/\mathcal{K}_\odot$  increases with the addition of DM. Therefore, we conclude that less massive star is more suitable for the detailed study of EoS. G3 is the softer EoS than the IOPB-I, which gives larger surface curvature than stiffer EoS both for the canonical and maximum mass star as given in Table 2. If the DM density is very high inside the NS, then the EoS becomes softer, which affects the curvatures significantly at the surface. The large curvature wrapped the space-time more than the smaller one. Using the Shapiro de-

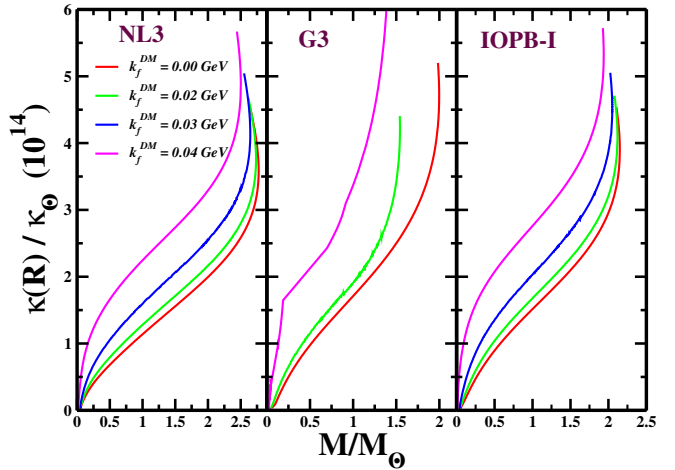


**Figure 6.** (colour online) The ratio of the surface curvature of NS and the Sun with the variation of NS mass with DM for NL3, G3 and IOPB-I.

lay measurement (Shapiro 1964), may one can find the NS using modern technology. Recently, the Shapiro effect has played an important role to test the GR in the strong-field regime of the NS using the binary pulsars (Pávásek 2019).

### 3.4 Binding energy of the NS

The gravitational binding energy (B) is defined as the mass difference between gravitational mass (M) and baryonic mass ( $M_B$ ) of the NS;  $B = M - M_B$ , where  $M$  is calculated as (Glen-dennning 1997; He et al. 2015)

$$M = \frac{1}{c^2} \int_0^R dr 4\pi r^2 \mathcal{E}(r), \quad (21)$$

and  $M_B = N m_b$ , where  $m_b$  is the mass of baryons (931.5 MeV/c $^2$ ) and  $N$  is the number of baryons calculated by the

volume integration over the whole radius in the Schwarzschild limit is

$$N = \int_0^R dr 4\pi r^2 \left[ 1 - \frac{2Gm(r)}{rc^2} \right]^{-1/2}. \quad (22)$$

The  $N$  is found to be  $\approx 10^{57}$  same as given in the Ref. Glen-denning (1997). We divide the  $B$  with the NS mass to form fractional  $B$ , which is  $B/M$  for easier to compare with our Sun. The binding energy per particle of the symmetric NM is  $\approx -16$  MeV, i.e. it needs 16 MeV to make the system unbound. For pure neutron matter (PNM) system, it is positive (Serot & Walecka 1986). That means the PNM system is already unstable. In the case of the NS, which consists of  $\approx 90\%$  of neutrons and  $\approx 10\%$  of protons and leptons. As we know, the nuclear force is state-dependent and the nucleon-nucleon interaction either singlet-singlet or triplet-triplet, which are repulsive (Patra & Praharaj 1992; Satpathy & Patra 2004; Kaur et al. 2020). However, the singlet-triplet nucleon-nucleon interaction is attractive. Due to the excess number of neutrons, the repulsive part adds instability to NS. As a result, the NS becomes unbound, which give positive binding of the system. However, its enormous gravitational force balanced the repulsive nuclear force. Thus for the whole NS, the  $B$  is negative.

With the addition of DM inside the NS, the  $B$  will going towards positive, that means it is going to be unstable. However, the instability of NS depends on the DM percentage. The variation of  $B/M$  with the variation of  $k_f^{DM}$  depicted in Fig. 7 for different parameter sets. The numerical values given in Table 2. The careful inspection of the Table 2 shows that up to the  $k_f^{DM}$  value 0.02 GeV the  $B$  of the canonical and maximum mass neutron star both are negative. That indicates that both the canonical and maximum mass neutron star system are bound systems with this amount of DM inside the system. However, as we increase the DM momentum, the canonical neutron star system becomes unbound with positive  $B$ . For example, with DM momentum 0.04 GeV the binding energy for the canonical star becomes positive for different parameter sets. But still, the maximum mass neutron star shows a bound system with negative binding energy. From this, we conclude that one can constraint the DM percentage inside the NS. If the DM percentage is more than canonical star, it forms a mini black hole at the core and destroys the NS (Goldman & Nussinov 1989; De Lavallaz & Fairbairn 2010; Kouvaris & Tinyakov 2011; Kouvaris 2012). The cooling of NS is also faster with the increasing of DM mass (Ding et al. 2019; Bhat & Paul 2020). That means the positive  $B$  may have a relation with the cooling properties of the NS or in other words; it may accelerate the urca process.

## 4 CONCLUSION

In the present work, we study the impacts of dark matter on the curvatures of the NS. The calculations are done with some well tested RMF parameters sets like NL3, the E-RMF parameter IOPB-I (two additional couplings to RMF) and G3 parameter (six extra couplings to RMF). The E-RMF formalism well suited to both finite nuclei properties as well as NM in extreme conditions. The parameter sets G3 and IOPB-I established the recently measured the maximum mass and the radius of the NS. The EoS of the NS is calculated

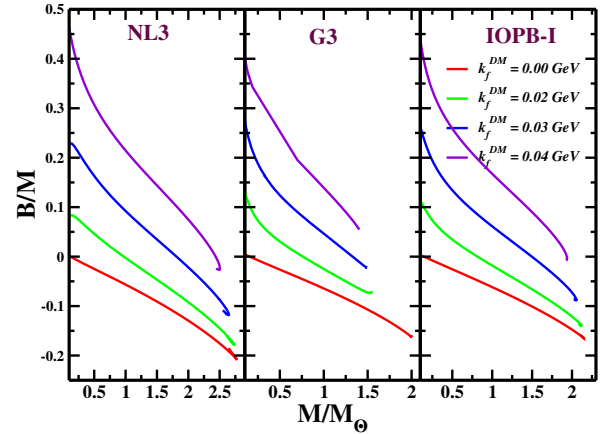


**Figure 7.** (colour online) The variation of  $B/M$  with the  $M/M_\odot$  of the NS with and without DM.

by assuming that the DM particles present inside the NS. We find that the DM effects play a significant role in the NS curvatures, even in the E-RMF model, which yield a softer EoS.

We calculate the various curvatures with the variations of the baryon density, mass and radius of the NS in the presence of the DM. The curvature increases or decreases with increase the baryon density. It is observed that at lower density the quantity  $\mathcal{K}$  and  $\mathcal{W}$  gives more curvature than  $\mathcal{J}$ ,  $\mathcal{R}$ . At the crust region, the curvatures  $\mathcal{J}$ , and  $\mathcal{R}$  almost vanish. The  $\mathcal{K}$  and  $\mathcal{W}$  approach each other within the crust and have a local maximum in that region. Moreover, the radial variation of  $\mathcal{K}(r)$  increases with the increasing DM momentum slowly up to canonical star and more for maximum star. The percental change of  $\mathcal{K}(r)$  with and without DM is approximately 33% for  $1.4 M_\odot$ , and it increases for the maximum mass star. From the surface curvature study, we conclude that the softer EoS gives large curvature than the stiffer one, which means the smaller massive star is more suitable to study the EoS of the NS. The binding energy increases towards positive with the increasing of DM momentum. From this, we conclude that a tiny amount of DM can accumulate inside the NS. The more percentage of the DM heat the NS, and it accelerates the urca process, which enhanced the cooling of the NS, and it makes the NS unstable.

## ACKNOWLEDGEMENTS

The computations is supported in part by the SAMKHYA: High Performance Computing Facility provided by Institute of Physics, Bhubaneswar. SKB is supported by the National Natural Science Foundation of China Grant No. 11873040

## REFERENCES

- Abbott B. P., et al., 2017, *Phys. Rev. Lett.*, 119, 161101
- Abbott B. P., et al., 2018, *Phys. Rev. Lett.*, 121, 161101
- Baldo M., Burgio G., 2016, *Progress in Particle and Nuclear Physics*, 91, 203–258
- Bethe H. A., 1971, *Annual Review of Nuclear Science*, 21, 93
- Bhat S. A., Paul A., 2020, *The European Physical Journal C*, 80, 544
- Bhuyan M., Patra S. K., 2012, *Mod. Phys. Lett. A*, 27, 1250173

Biswal S. K., Singh S. K., Bhuyan M., Patra S. K., 2015, *Brazilian Journal of Physics*, 45, 347–352

Carroll S. M., 2019, *Spacetime and Geometry: An Introduction to General Relativity*. Cambridge University Press

Ciarcelluti P., Sandin F., 2011, *Phys. Lett. B*, 695, 19–21

Cromartie H. T., et al., 2019, *Nature Astronomy*, 4, 72–76

Danielewicz P., Lee J., 2014, *Nucl. Phys. A*, 922, 1

Das A., Malik T., Nayak A. C., 2019, *Phys. Rev. D*, 99, 043016

Das H. C., Kumar A., Kumar B., Biswal S. K., Nakatsukasa T., Li A., Patra S. K., 2020, *MNRAS*, 495, 4893

De Lavallaz A., Fairbairn M., 2010, *Phys. Rev. D*, 81, 123521

Ding W.-B., Yu Z., Xu Y., Liu C.-J., Bao T., 2019, *Chin. Phys. Lett.*, 36, 049701

Ekşioğlu K. Y., Güngör C., Türkoglu M. M., 2014, *Phys. Rev. D*, 89, 063003

Ellis J., Hüttsi G., Kannike K., Marzola L., Raidal M., Vaskonen V., 2018, *Phys. Rev. D*, 97, 123007

Emspak J., 2017, What the Neutron Star Collision Means for Dark Matter, <https://www.smithsonianmag.com/author/jesse-emspak/>

Furnstahl R. J., Price C. E., Walker G. E., 1987, *Phys. Rev. C*, 36, 2590

Furnstahl R. J., Serot B. D., Tang H.-B., 1997, *Nucl. Phys. A*, 615, 441

Garg U., Colařík G., 2018, *Progress in Particle and Nuclear Physics*, 101, 55

Glendenning N. K., 1997, *Compact stars: Nuclear physics, particle physics, and general relativity*. Springer-Verlag New York

Goldman I., Nussinov S., 1989, *Phys. Rev. D*, 40, 3221

GAjver T., Erkoca A. E., Reno M. H., Sarcevic I., 2014, *Journal of Cosmology and Astroparticle Physics*, 2014, 013

Harada T., 1998, *Phys. Rev. D*, 57, 4802

He X.-T., Fattoyev F. J., Li B.-A., Newton W. G., 2015, *Phys. Rev. C*, 91, 015810

Horowitz C. J., Piekarewicz J., 2001, *Phys. Rev. Lett.*, 86, 5647

Horowitz C. J., et al., 2014, *Journal of Physics G: Nuclear and Particle Physics*, 41, 093001

Ivanytskyi O., Sagun V., Lopes I., 2019 ([arXiv:1910.09925](https://arxiv.org/abs/1910.09925))

Joglekar A., Raj N., Tanedo P., Yu H.-B., 2019 ([arXiv:1911.13293](https://arxiv.org/abs/1911.13293))

Kaur M., Quddus A., Kumar A., Bhuyan M., Patra S. K., 2020, *Journal of Physics G: Nuclear and Particle Physics*

Kouvaris C., 2008, *Phys. Rev. D*, 77, 023006

Kouvaris C., 2012, *Phys. Rev. Lett.*, 108, 191301

Kouvaris C., Tinyakov P., 2010, *Phys. Rev. D*, 82, 063531

Kouvaris C., Tinyakov P., 2011, *Phys. Rev. D*, 83, 083512

Kumar B., Singh S., Agrawal B., Patra S., 2017, *Nuclear Physics A*, 966, 197

Kumar B., Patra S. K., Agrawal B. K., 2018, *Phys. Rev. C*, 97, 045806

Lalazissis G. A., König J., Ring P., 1997, *Phys. Rev. C*, 55, 540

Lattimer J. M., Prakash M., 2004, *Science*, 304, 536

Lattimer J. M., Prakash M., 2007, *Phys. Reports*, 442, 109

Leung S.-C., Chu M.-C., Lin L.-M., 2011, *Phys. Rev. D*, 84, 107301

Li A., Huang F., Xu R.-X., 2012, *Astroparticle Phys.*, 37, 70–74

Li B.-A., Krastev P. G., Wen D.-H., Zhang N.-B., 2019, *EPJ A*, 55

Martin S. P., 1998, A Supersymmetry Primer. pp 1–98

Miller L. D., Green A. E. S., 1972, *Phys. Rev. C*, 5, 241

MAjiller H., Serot B. D., 1996, *Nuclear Physics A*, 606, 508

Oppenheimer J. R., Volkoff G. M., 1939, *Phys. Rev.*, 55, 374

Panotopoulos G., Lopes I., 2017, *Phys. Rev. D*, 96, 083004

Patra S. K., Praharaj C. R., 1992, *Europhysics Letters (EPL)*, 20, 87

Psaltis D., 2008, *Living Rev. Relativ.*, 11, 9

PÄüssel M., 2019 ([arXiv:2001.00229](https://arxiv.org/abs/2001.00229))

Quddus A., Panotopoulos G., Kumar B., Ahmad S., Patra S. K., 2020, *Journal of Physics G: Nuclear and Particle Physics*

Rashdan M., 2001, *Phys. Rev. C*, 63, 044303

Reinhard P. G., 1988, *Z. Phys. A Atomic Nuclei*, 329, 257

Ring P., 1996, *Progress in Particle and Nuclear Physics*, 37, 193

Rosi G., Cacciapuoti L., Sorrentino F., Menchetti M., Prevedelli M., Tino G. M., 2015, *Phys. Rev. Lett.*, 114, 013001

Ruppin F., Billard J., Figueroa-Feliciano E., Strigari L., 2014, *Phys. Rev. D*, 90, 083510

Sandin F., Ciarcelluti P., 2009, *Astroparticle Phys.*, 32, 278–284

Satpathy L., Patra S. K., 2004, *Journal of Physics G: Nuclear and Particle Physics*, 30, 771

Serot B. D., Walecka J. D., 1986, *Adv. Nucl. Phys.*, 16, 1

Shapiro I. I., 1964, *Phys. Rev. Lett.*, 13, 789

Shapiro S., Teukolsky S., 1983, *Black holes, white dwarfs, and neutron stars: The physics of compact objects*. John Wiley & Sons, Ltd

Sharma B. K., Centelles M., Viñas X., Baldo M., Burgio G. F., 2015, *A&A*, 584, A103

Singh S. K., Biswal S. K., Bhuyan M., Patra S. K., 2014, *Journal of Physics G: Nuclear and Particle Physics*, 41, 055201

Sotani H., 2014, *Phys. Rev. D*, 89, 104005

Sugahara Y., Toki H., 1994, *Nuclear Physics A*, 579, 557

Tolman R. C., 1939, *Phys. Rev.*, 55, 364

Tsang M. B., Zhang Y., Danielewicz P., Famiano M., Li Z., Lynch W. G., Steiner A. W., 2009, *Phys. Rev. Lett.*, 102, 122701

Walecka J., 1974, *Ann. Phys.*, 83, 491

Will C. M., 2014, *Living Reviews in Relativity*, 17, 4

Xiang Q.-F., Jiang W.-Z., Zhang D.-R., Yang R.-Y., 2014, *Phys. Rev. C*, 89, 025803

Xu C., Li B.-A., Chen L.-W., 2010, *Phys. Rev. C*, 82, 054607

Zimmerman J., Carson Z., Schumacher K., Steiner A. W., Yagi K., 2020 ([arXiv:2002.03210](https://arxiv.org/abs/2002.03210))

Zyla P., Barnett R., Beringer J., et al. 2020, Particle Data Group, [http://pdg.lbl.gov/2020/html/authors\\_2020.html](http://pdg.lbl.gov/2020/html/authors_2020.html)